Crystal fields of porphyrins and phthalocyanines from polarization-dependent 2p-to-3d multiplets

Johnson, Phillip S.; García Lastra, Juan Maria; Kennedy, Colton K.; Jersett, Nathan J.; Boukahil, Idris; Himpsel, F. J.; Cook, Peter L.

Published in:
Journal of Chemical Physics

Link to article, DOI:
10.1063/1.4868552

Publication date:
2014

Document Version
Publisher's PDF, also known as Version of record

Crystal fields of porphyrins and phthalocyanines from polarization-dependent 2p-to-3d multiplets

Phillip S. Johnson, J. M. García-Lastra, Colton K. Kennedy, Nathan J. Jersett, Idris Boukahil, F. J. Himpsel, and Peter L. Cook

Citation: The Journal of Chemical Physics **140**, 114706 (2014); doi: 10.1063/1.4868552
View online: http://dx.doi.org/10.1063/1.4868552
View Table of Contents: http://scitation.aip.org/content/aip/journal/jcp/140/11?ver=pdfcov
Published by the AIP Publishing

Crystal fields of porphyrins and phthalocyanines from polarization-dependent 2p-to-3d multiplets

Phillip S. Johnson,[1] J. M. García-Lastra,[2] Colton K. Kennedy,[3] Nathan J. Jersett,[3] Idris Boukahil,[1] F. J. Himpsel,[1,a)] and Peter L. Cook[3]
[1]*Department of Physics, University of Wisconsin-Madison, 1150 University Ave., Madison, Wisconsin 53706, USA*
[2]*Department of Energy Conversion and Storage, Technical University of Denmark, 4000 Roskilde, Denmark*
[3]*Natural Sciences Department, University of Wisconsin-Superior, Belknap and Catlin, Superior, Wisconsin 54880, USA*

(Received 6 December 2013; accepted 3 March 2014; published online 20 March 2014)

Polarization-dependent X-ray absorption spectroscopy is combined with density functional calculations and atomic multiplet calculations to determine the crystal field parameters 10Dq, Ds, and Dt of transition metal phthalocyanines and octaethylporphyrins (Mn, Fe, Co, Ni). The polarization dependence facilitates the assignment of the multiplets in terms of in-plane and out-of-plane orbitals and avoids ambiguities. Crystal field values from density functional calculations provide starting values close to the optimum fit of the data. The resulting systematics of the crystal field can be used for optimizing electron-hole separation in dye-sensitized solar cells. © *2014 AIP Publishing LLC*. [http://dx.doi.org/10.1063/1.4868552]

I. INTRODUCTION

In order to systematically design dye molecules for solar cells with optimized sunlight absorption and charge separation, it is important to control their energy levels together with the driving forces that separate electrons and holes. Typical dye molecules, such as porphyrins and phthalocyanines, contain a central 3d or 4d metal ion surrounded by an organic π system. In previous work we have used a combination of X-ray absorption spectroscopy (XAS) and first principles density functional theory (DFT) calculations to systematically investigate their energy level structure,[1,2] to detect the influence of axial and peripheral ligands on the energy levels,[3] to compare the level structure of Ru- and Fe-based dye molecules,[4] and to investigate the energy levels in different parts of donor-π-acceptor complexes.[5] There is a substantial amount of literature on the characteristic multiplet structure of the metal 2p-to-3d transitions in such molecules.[6–15] For Mn see Refs. 16 and 17; for Fe, Refs. 18–26; for Co, Ref. 27; for Ni, Ref. 28; for Cu, Refs. 29 and 30; for Zn, Ref. 31. TiO-Pcs[3,32] and VO-Pcs[33,34] have also been studied as possible dye molecules.

Here we focus on the crystal field generated by the negatively charged N atoms surrounding the central metal ion of porphyrins and phthalocyanines. Usually, the HOMO is located at the metal atom and the LUMO is delocalized over the N atoms and the surrounding π-system. This results in optical transitions with charge-transfer character, which start the separation of electrons and holes. The crystal field then can either assist charge separation or suppress it. In both cases it is important to know its sign and magnitude to find ways of steering the carriers in the right direction.

The crystal field parameters of π-bonded, square planar transition metal complexes such as phthalocyanines and porphyrins are difficult to obtain from UV-visible absorption spectra, since the d-d electronic transitions are masked by stronger π-π^* transitions, as well as metal-ligand or ligand-metal charge transfer bands.[35–37] As a result, a search for published values of crystal field parameters from optical spectroscopy did not produce any results for the molecules investigated here. As stated in a review of UV-visible absorption spectra of phthalocyanines and porphyrins:[35] "Despite the large number of spectra that have been measured and analyzed since the 1970s, a complete model that could accurately account for all optical properties of even just the $\pi \rightarrow \pi^*$ and n $\rightarrow \pi^*$ transitions of the phthalocyanine ring is not available."

Our approach is based on the fine structure of the 2p-to-3d core-to-valence transitions of the 3d transition metal series. These transitions are highly dipole selective toward 3d final states, thereby eliminating competing transitions involving π^* orbitals. The multiplet structure reveals both the crystal field at the transition metal atom and the Coulomb interaction between its 3d electrons. This has been amply demonstrated in previous work,[21,38,39] and codes have been developed to calculate the full multiplet structure originating from the crystal field plus the Coulomb/exchange interaction between the 3d valence electrons and the 2p core hole.[38–40]

In addition, we use the polarization dependence of the multiplet intensities from molecular films oriented by the substrate (compare Refs. 8, 9, 11, 12, 18, 25, 27, 29, and 41). This doubles the experimental information and strongly constrains the crystal field parameters. The extra information is particularly important when going from the frequently studied octahedral O_h symmetry to planar molecules with lower symmetry, here D_{4h}. These require two additional parameters Ds and Dt in addition to the octahedral crystal field parameter 10Dq, which generate many possible combinations including

a)Electronic mail: fhimpsel@wisc.edu

false minima. Even with the extra polarization information, the high sensitivity of the multiplet structure to small deviations in the crystal field parameters and to the assumed ground state requires extra information for a unique fit. We found it highly advantageous to have DFT calculations for several exchange/correlation potentials available to obtain reliable starting values of the crystal field parameters.

As a result of the combined XAS and DFT study we present systematic crystal field parameters for phthalocyanines and octaethylporphyrins involving the transition metals from Mn though Ni. These provide the starting point for designing dye molecules that optimally separate electrons and holes via the crystal field.

II. EXPERIMENTAL

A. Sample preparation and characterization

Iron(II) phthalocyanine (Fe-Pc), cobalt(II) phthalocyanine (Co-Pc), nickel(II) phthalocyanine (Ni-Pc), manganese (III) octaethylporphyrin chloride (MnCl-OEP), cobalt(II) octaethylporphyrin (Co-OEP), and nickel(II) octaethylporphyrin (Ni-OEP) were purchased from Sigma-Aldrich and used as received. In order to obtain the best quality spectra (with the narrowest peaks and largest peak-to-valley ratios), the molecules in this study were outgassed and sublimed *in situ* onto either Si substrates with native oxide or Au. Sublimation of these molecules also ensured that they were in the appropriate oxidation state by removing adsorbates loosely bound to the metal atom. Sublimation temperatures (to within 10 °C) were 445 °C for Fe-Pc, 460 °C for Co-Pc and Ni-Pc, and 250 °C for Co-OEP and Ni-OEP. Mn-OEP was prepared by sublimation of MnCl-OEP at 455 °C, above the typical OEP evaporation temperature of 250 °C. At this higher temperature, the axial Mn-Cl bond was broken for most of the molecules and Cl desorbed. Sample integrity was monitored by checking N 1s spectra of each sample for a characteristic peak just below 400 eV which corresponds to a broken phthalocyanine or porphyrin ring.[4] No such peaks were observed for the sublimed samples. Typical N 1s spectra are shown in Figure 1 and the supplementary material.[55]

The polarization dependence of the N 1s spectra of Fe(II)-Pc in Fig. 1 provides quantitative information about the orientation of the deposited films.[1,9,12,13,18,25] The N 1s edge of transition metal phthalocyanines is influenced by the nature of the central metal atom,[42] but we do not focus on these effects here as they do not strongly affect the use of the N 1s edge as a probe of molecular orientation. Well-ordered films were obtained on Si wafers covered with the native oxide, a widely used substrate. In that case the Pc molecules were preferentially oriented with their molecular planes perpendicular to the substrate and the OEP molecules parallel to it. The film thickness played a role in optimizing the polarization dependence. Typically, the best polarization dependence is seen in films a few layers thick, but not thick enough to be visible (compare Ref. 41). Films with visible color still show polarization dependence in their spectra, but it is reduced compared to thinner samples because of disorder from surface nonuniformity. Polarization-dependent N 1s spectra for Co(II)-Pc, Co(II)-OEP, Ni(II)-Pc, and Ni(II)-OEP can be found in the supplementary material.[55] The supplementary material also contains plots of the LUMO peak intensity versus $\cos^2\theta$. The slope of these curves is a measure of the degree of orientation. For Au substrates the polarization dependence was much weaker, as shown in the bottom half of Fig. 1. A likely explanation for the disorder present in the films on air-exposed Au substrates is their inhomogeneous nature. While the initial few layers are well-ordered and lie flat on a clean surface, additional layers see a much rougher surface which causes them to stand on edge.[41] Therefore the silicon substrates with their native oxide were chosen for determining the crystal field parameters. They also more closely resemble substrates in actual devices.

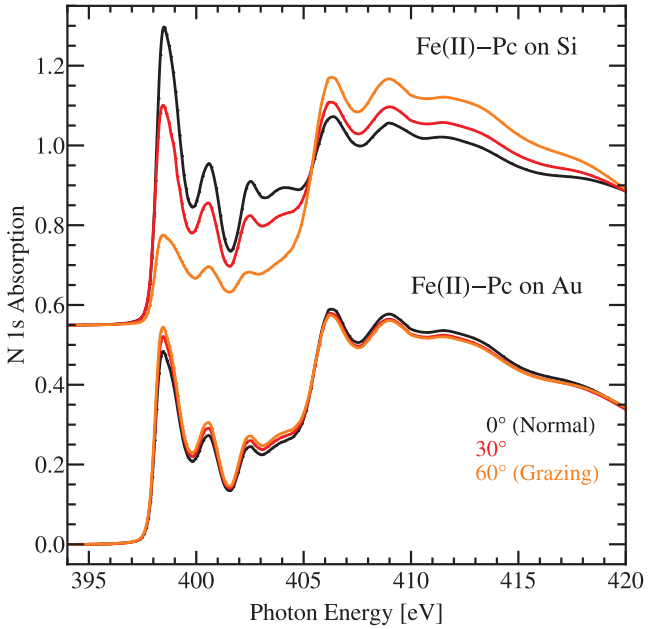

FIG. 1. N 1s spectra of Fe(II)-Pc sublimed onto oxidized Si and Au substrates. The polarization dependence of the spectra indicates that Fe(II)-Pc stands up on Si and has nearly random orientation on Au. Therefore Si substrates were chosen for determining the crystal field parameters of the molecules.

B. X-ray absorption measurements

X-ray absorption measurements for all molecules were performed at the U2 VLS-PGM beamline at the Synchrotron Radiation Center (SRC). Additional measurements of Ni(II)-Pc for higher resolution spectra were performed at Beamline 8.0 at the Advanced Light Source (ALS). All spectra were taken in the surface-sensitive total electron detection mode. The energy calibration of the metal 2p spectra was based on published data.[1] The N 1s spectra were calibrated as in Ref. 4. Radiation damage was minimized by using the narrowest possible exit slits. The absolute accuracy is about ±0.2 eV, the relative accuracy for the same edge of different compounds about ±0.1 eV, and the relative accuracy within a spectrum about ±0.05 eV. For fitting the 2p-to-3d transitions, we eliminated the small 2p-to-s continuum by subtracting an integral curve of the spectrum with a pre-factor such that the base line returned to 0 above the 3d transitions.

C. Density functional theory

DFT calculations were performed by means of the Amsterdam Density Functional (ADF) code, version 2012.01 (Ref. 43). All atoms were described through basis sets of triple-ζ polarized quality (triple-ζ Slater-type orbital (STO) plus one polarization function) given in the program database, including all the core electrons in the calculation (i.e., with no frozen core approximation). Spin-polarized calculations were carried out using three levels of approximation for the exchange-correlation potential, namely: (i) local density approximation (LDA) employing the Vosko-Wilk-Nusair (VWN) functional,[44] (ii) general gradient approximation (GGA) using the Perdew-Burke-Ernzerhof (PBE) functional,[45] (iii) a hybrid scheme mixing GGA and exact Hartree-Fock exchange with the so-called BHandHLYP functional.[43] In a first step we calculated the ground state geometries of all the compounds studied in the present work. The corresponding occupations of the d-orbitals for the ground state of each compound are the following: (i) Ni(II)-Pc and Ni(II)-OEP $[(xy)^2\ (xz)^2\ (yz)^2\ (3z^2 - r^2)^2\ (x^2 - y^2)^0]$; (ii) Co(II)-Pc and Co(II)-OEP $[(xy)^2\ (xz)^2\ (yz)^2\ (3z^2 - r^2)^1\ (x^2 - y^2)^0]$; (iii) Fe(II)-Pc $[(xy)^2\ (xz)^1\ (yz)^1\ (3z^2 - r^2)^2\ (x^2 - y^2)^0]$; (iv) Mn(II)-OEP $[(xy)^1\ (xz)^1\ (yz)^1\ (3z^2 - r^2)^1\ (x^2 - y^2)^1]$. Second we used an "Average of Occupations" (AOC) procedure to evaluate the corresponding crystal field parameters of each system. In the AOC procedure the d-electrons are equally distributed over the five d-orbitals (e.g., for Ni-Pc the occupations were $(xy)^{1.6}\ (xz)^{1.6}\ (yz)^{1.6}\ (3z^2 - r^2)^{1.6}\ (x^2 - y^2)^{1.6}$), while the geometry of the molecule was fixed to that of the ground state. Crystal field parameters could then be obtained simply by taking the Kohn-Sham energies of the d-orbitals. This AOC technique has been shown to be accurate for the crystal field splitting of many other transition metal complexes.[46,47]

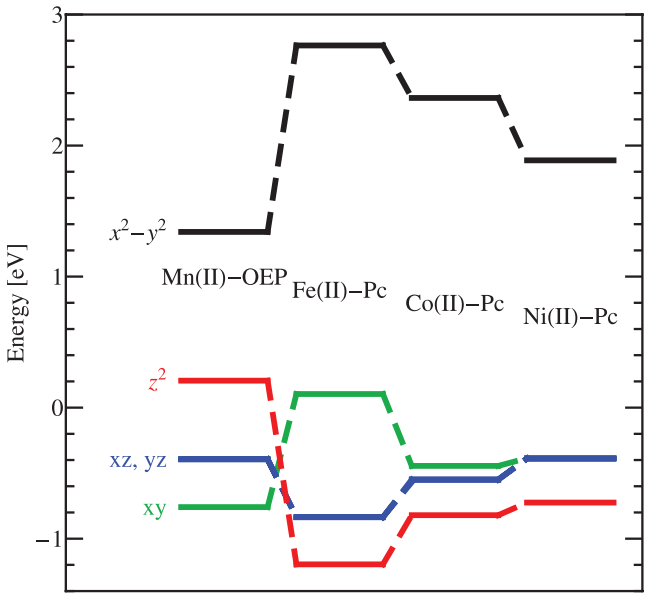

FIG. 2. One-electron energy levels for the 3d electrons in Mn-OEP, Fe-Pc, Co-Pc, Ni-Pc, obtained from the optimized crystal field parameters in Table II. In addition to the crystal field, one must take into account the electron-electron interaction for determining the total energy and the ground state.

The crystal field parameters 10Dq, Ds, and Dt can be used to calculate the 3d manifold in the one-electron picture,[3,48] as shown in Figure 2. We do not include the electron occupancy of the orbitals here, because the crystal field is not the only factor determining the total energy versus occupancy. The Coulomb/exchange energy among the 3d electrons is at least as important. There also remain some questions regarding the ground state configurations of Pcs, particularly Fe(II)-Pc.[6–11,13,19–22,24] The octahedral crystal field 10Dq splits the 3d level into a doubly degenerate e_g level and a triply degenerate t_{2g} level, both of which are then split further by the tetragonal distortion of the crystal field in planar, four-fold molecules. For Figure 2 we have already used the fully-optimized parameters, thereby providing an overview of the results from our work. Since the Coulomb/exchange interaction between the 3d electrons is comparable to the crystal field splitting, care has to be taken not to overinterpret such diagrams. For example, the actual multiplets consist of typically 10-100 lines with varying parentage (see the discussion below). They reflect many-electron states which cannot be represented in a single-electron picture. Nevertheless, the one-electron picture has been used widely as a first approximation to describe 3d-levels in transition metal oxides.

D. Multiplet calculations and fitting

Before getting into the details of calculating the observed 2p-to-3d multiplets, it is worth discussing their connection with the crystal field, both in the ground state and the excited state. The 2p core hole introduces a major perturbation in the 3d electron manifold by its extra positive charge (which lowers all the 3d levels) and by its Coulomb/exchange interactions with the 3d electrons. In addition, an extra 3d electron is generated by the optical absorption process, which interacts with all the other 3d electrons. Despite these radical changes in the 3d manifold, the crystal field is not affected much, because it is caused by charges on the neighboring N atoms. In fact, the absorption of visible light in a solar cell also generates an extra electron, which makes the crystal field obtained from X-ray absorption spectroscopy more realistic than the ground state crystal field, as far as photovoltaics are concerned.

Fits of the 2p-to-3d absorption spectra are performed using the CTM4XAS atomic multiplet code.[39] Generally, a uniform reduction of the calculated crystal field parameters and Slater integrals for the Coulomb/exchange interaction provides a fairly direct route to a best fit. This is an indication that DFT calculations tend to obtain the correct ratio of the various interactions, but have difficulties describing the screening quantitatively.

Specifically, the observed $2p_{3/2}$ to 3d multiplets are calculated from the three crystal field parameters in D_{4h} symmetry, 10Dq, Ds, and Dt, together with atomic Slater integrals using CTM4XAS,[39] which is based on Cowan's atomic multiplet code[49] with modifications by Butler,[50] Thole *et al.*,[21] and Ogasawara *et al.*[51] As an example, the Fe(II)-Pc spectra corresponding to the crystal fields obtained from the three DFT

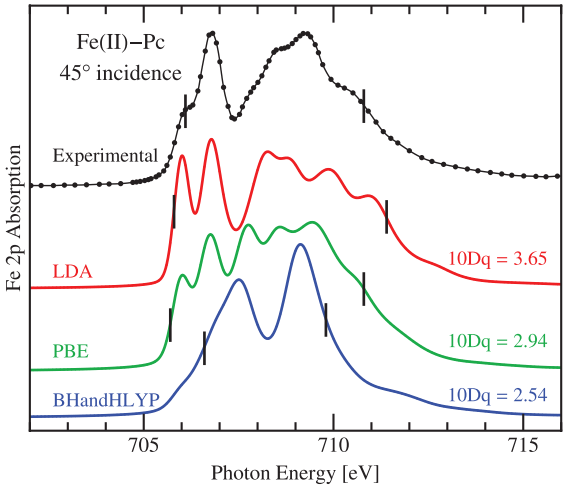

FIG. 3. Comparison of the experimental spectrum of Fe(II)-Pc at 45° incidence and calculated spectra using several different functionals (see Table I for details). Black lines indicate the FWHM of the $2p_{3/2}$ region and show how 10Dq influences the overall width by splitting the 3d-level. The PBE functional provides the most accurate width and is used as the starting point for optimizing the crystal field parameters.

functionals are shown in Figure 3. The corresponding parameters are given in Table I. The Slater parameter was set to 1 for all spectra.

There are substantial differences between the functionals, which can be traced to different values of the dominant crystal field parameter 10Dq. As the crystal field increases, the full width half maximum of the $2p_{3/2}$ manifold increases, which is indicated by tick marks in Fig. 3. Comparing the widths of the calculated spectra with the experimental width, the PBE functional comes closest to the data, an observation that holds for the other molecules as well. To obtain optimal fits, the PBE crystal field parameters need to be reduced slightly. This was corrected by uniformly reducing all crystal field parameters for each molecule (typically between 5% and 30%). In some cases it was necessary to fine tune the ratios of the crystal field parameters (in particular to move the third peak of the PBE spectrum in Fig. 3 to higher energy), but we kept such deviations from the calculated ratios to a minimum.

The rationale for this strategy was that DFT calculations do not account completely for screening which reduces electrostatic interactions. The Slater integrals could be affected by the localization of the 3d states in the presence of the core hole, as discussed previously.[52,53] The degree of covalency together with the appearance of ligand holes may also be a factor. Therefore we investigated the rescaling of the Slater parameters and the crystal field parameters independently of each other. The corresponding figures are included in the supplementary material.[55] These figures also establish the margins of error for the crystal field and Slater parameters.

TABLE I. Crystal field parameters for Fe-Pc produced by several different functionals, Fig. 3.

Functionals	10Dq	Dt	Ds
LDA	3.65	0.329	0.608
PBE	2.94	0.257	0.597
BHandHLYP	2.54	0.237	0.446

More generally, a core level transition represents a highly excited state, which raises the question of how much the presence of the core hole distorts the ground state electronic structure of the valence electrons. The presence of the core hole is included in the multiplet calculations,[49] but the localization of the 3d-electrons induced by the 2p core hole will affect the Slater parameters. The crystal field is affected less by the core hole, since it originates from neighboring N atoms, not the metal itself. It would be desirable to have crystal field parameters available from UV-visible spectroscopy, where the core hole is absent. These are difficult to obtain due to the dominance of transitions involving π levels.[35–37] There are optical data available for octahedral Mn complexes that do not contain π orbitals. A comparison with core level absorption[52] shows a reduction of 10Dq by about 0.2 eV in the presence of a core hole.

In order to model the polarization dependence of the spectra, it is important to appropriately scale the oscillator strengths of the in-plane and out-of-plane transitions produced by the multiplet calculations. The Pc and OEP molecules were found to have orientations roughly orthogonal to each other on oxidized Si substrates. Therefore we calculated the polarization dependence for two different orientations of the planar molecules: one for lying on edge, the other for lying flat. For molecules lying on edge, the intensity of the spectrum at a given energy is

$$I_{\perp} = \frac{1}{2}[Z\cos^2\theta + R(2 - \cos^2\theta)], \tag{1}$$

where Z is the oscillator strength of the out-of-plane transitions, R is the oscillator strength of the in-plane transitions (note that for our purposes R and L polarizations are identical), and θ is the angle of incidence measured from normal to the substrate. For molecules lying flat one obtains

$$I_{\parallel} = Z(1 - \cos^2\theta) + R\cos^2\theta, \tag{2}$$

with the same assignments. In each case it is assumed that the molecules are azimuthally disordered but with no tilt from either normal or parallel to the surface, respectively.

The difference between the two situations can be rationalized by considering the available transitions at normal (0°) and extreme grazing (90°) X-ray incidence. At normal incidence, both in-plane and out-of-plane transitions are allowed for azimuthally disordered molecules lying on edge, while molecules lying flat exhibit only in-plane transitions. At grazing incidence the allowed transitions are only in-plane for molecules lying on edge and out-of-plane transitions for molecules lying flat. Between these extreme cases the oscillator strengths have the $\cos^2\theta$ dependence of optical dipole transitions.

III. RESULTS

The calculated spectra in Figs. 4–8 come from multiplet calculations using the optimized crystal field and Slater parameters in Table II. The polarization dependence was obtained from the CTM4XAS intensities R and Z via Eqs. (1)

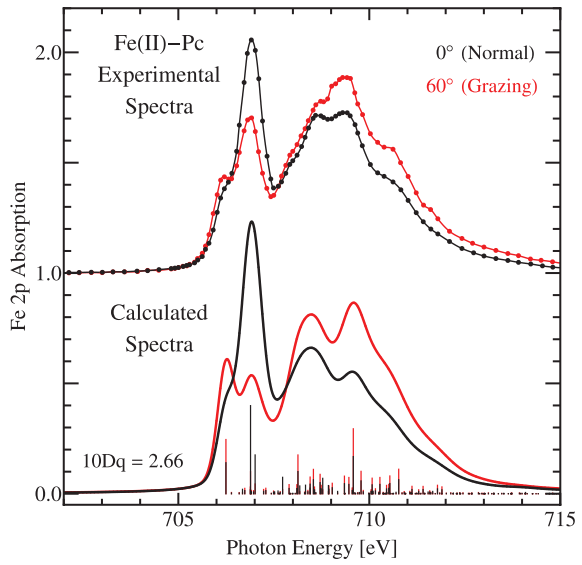

FIG. 4. Comparison of experimental and calculated spectra for Fe(II)-Pc at normal and grazing incidence. The peak energies are reproduced in the calculated spectra, but the experimental polarization dependence is smaller due to imperfect orientation. Features seen strongly at normal incidence have out-of-plane symmetry, and those stronger at grazing incidence in-plane symmetry.

and (2). Each transition is simulated by a Voigt profile with area equal to the oscillator strength calculated by CTM4XAS and linearly increasing broadening going to higher energies. The calculated spectra assume that the molecules are perfectly ordered and oriented exactly normal (for Pcs) or parallel (for OEPs) to the surface. They will thus exhibit stronger polarization dependence than the experimental spectra, which are somewhat disordered and tilted from normal or parallel orientations. The lines under the calculated spectra indicating transition oscillator strengths are scaled for their respective angles of incidence. The strong calculated polarization dependence shows that for a perfectly ordered film aligned perpendicular (for Pcs) or parallel (for OEPs) to the substrate, a much more dramatic effect could be observed.

The metal 2p absorption edges determine the crystal field, and the polarization dependence of the spectra is particularly important for uniquely determining the crystal field parameters. Figure 4 compares Fe $2p_{3/2}$ absorption spectra for Fe(II)-Pc with atomic multiplet calculations for two polarizations (red and black). The Fe $2p_{1/2}$ region is omitted because its features are not as well defined. Overall, theory and experiment exhibit similar multiplet structures with comparable polarization dependence. The peak near 707 eV is strongest at normal incidence, which indicates that the corresponding 3d orbitals have an out-of-plane orientation, because the Pc molecules lie on edge according to the N 1s data in Fig. 1 and the supplementary material.[55] A secondary peak on the lower energy side of the main peak has opposite polarization dependence and thus corresponds to an orbital with in-plane symmetry. The higher energy peaks likewise have opposite polarization dependence corresponding to 3d orbitals with in-plane orientation. The modulation of the spectra in this region is reduced compared to the modulation at lower energies. The symmetries of the transitions in these spectra are consistent with a previously reported spin 1 ground state[6–11,13,19–22,24]

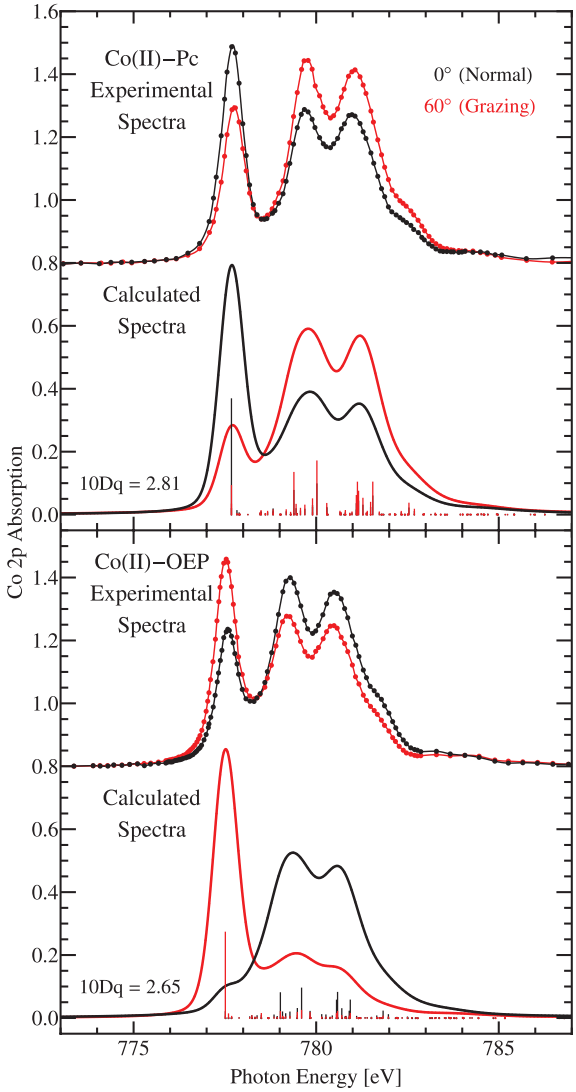

FIG. 5. Experimental and calculated Co 2p absorption spectra for Co(II)-Pc and Co(II)-OEP. Pc and OEP films have opposite polarization dependence, indicating that Pcs preferentially stand on edge while OEPs lie flat. Compared to Fe(II)-Pc, the lower number of unoccupied 3d states reduces the number of strong transitions in the multiplet.

which leaves the $d_{xz, yz}$, and d_{xy} orbitals partially filled, thus transitions into each are allowed. While there remain questions over the electron occupancy of the ground state of the Fe^{2+} ion in Fe(II)-Pc, the polarization dependence seen in these spectra potentially offers clues to the available orbitals in the excited state.

The same polarization dependence pattern can be seen in the Co $2p_{3/2}$ spectra of Co(II)-Pc in Figure 5 (top panel). Again the low-energy peak is strong at normal incidence, and the higher-lying peaks are strong at grazing incidence. The total number of transitions in Co-Pc spectra is lower than for Fe-Pc because of the extra d electron in the Co^{2+} ground state. Thus fewer unoccupied levels are available for the excited electron, notably the loss of the lower energy shoulder on the dominant peak and fewer transitions in the higher energy region. The ground state of Co^{2+} in these molecules is spin $\frac{1}{2}$.[6–8,10,11,13,27] Co 2p spectra of Co(II)-OEP are also shown in the bottom panel of Figure 5. They have similar

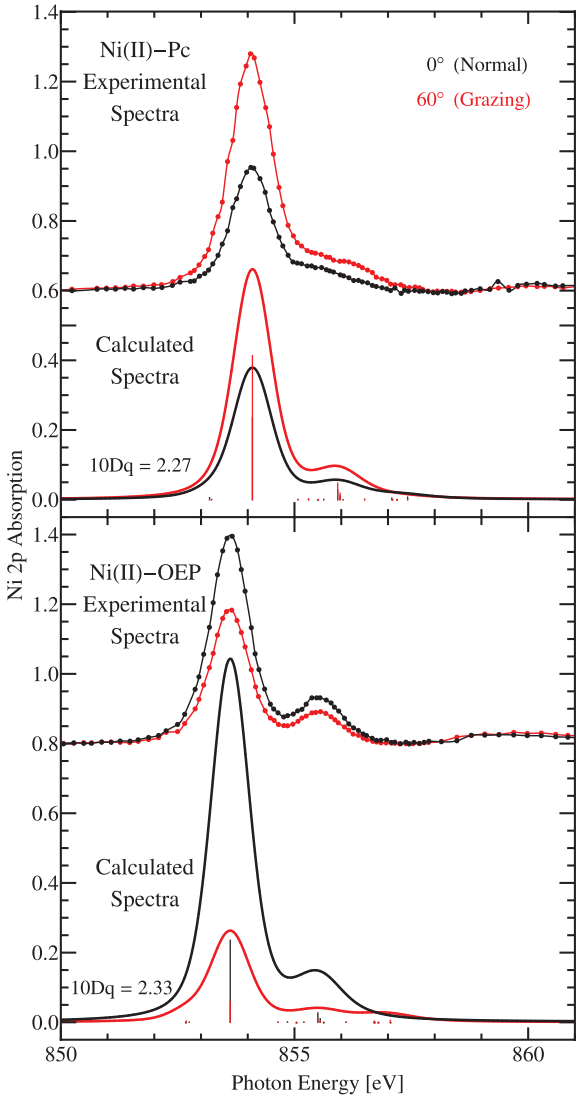

FIG. 6. Experimental and calculated Ni 2p absorption spectra for Ni(II)-Pc and Ni(II)-OEP. As with Co(II)-Pc and Co(II)-OEP, the Pc and OEP have opposite polarization dependence. For Ni(II)-Pc and Ni(II)-OEP all 3d levels except for the highest lying e_g level are occupied, such that all transitions have the same polarization dependence. They correspond to the higher energy transitions in Figures 4 and 5.

multiplet structure to Co(II)-Pc but opposite polarization dependence. This is in line with the opposite orientation of OEP compared to Pc molecules observed at the N 1s edge in the supplementary material.[55] OEP lies flat on the SiO_2 substrate rather than on edge.

In the Ni $2p_{3/2}$ spectra of Figure 6 the multiplet is reduced to a single, dominant line with weak features at higher energy (compare Fig. 7 for a higher resolution spectrum measured at the ALS). This continues the trend towards fewer available empty levels when going from Fe to Co and Ni. In Ni, only the highest-lying e_g level remains unoccupied and thus dominates the spectra. The polarization dependence of this peak is opposite to that of the low-energy peak of the Fe 2p and Co 2p spectra in Figs. 4 and 5. This is because the out-of-plane d_{xz} and d_{yz} orbitals have now become filled[6–8,28] (thus Ni^{2+} has a spin 0 ground state), leaving only the in-plane $d_{x^2-y^2}$ orbital available for the excited 3d electron (see Fig. 2). The dominant Ni 2p transition thus corresponds to the higher energy transitions in the Fe 2p and Co 2p spectra. The orientation of the molecules has not changed according to the N 1s spectra in the supplementary material,[55] as expected. Ni-Pc and Ni-OEP spectra have again opposite polarization dependence, which is consistent with their opposite orientation. The high-resolution spectrum in Fig. 7 shows a clearly-resolved doublet above the main peak for Ni-Pc, which is just a single peak at 855.5 eV in Ni-OEP (Fig. 6) and in the multiplet calculation. This is in agreement with previous work.[1,28] The splitting is not un-

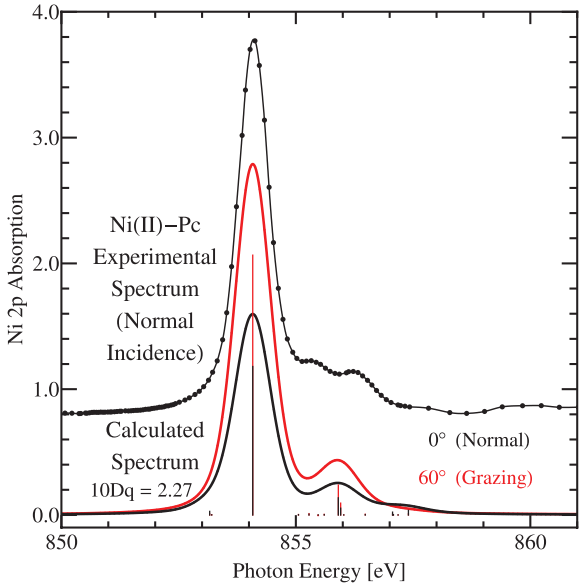

FIG. 7. Higher resolution spectrum from a thicker sample of Ni(II)-Pc, which showed lower polarization dependence. The calculation shows a single peak above the main peak (as in Ni-OEP), which is split in the experimental spectrum.

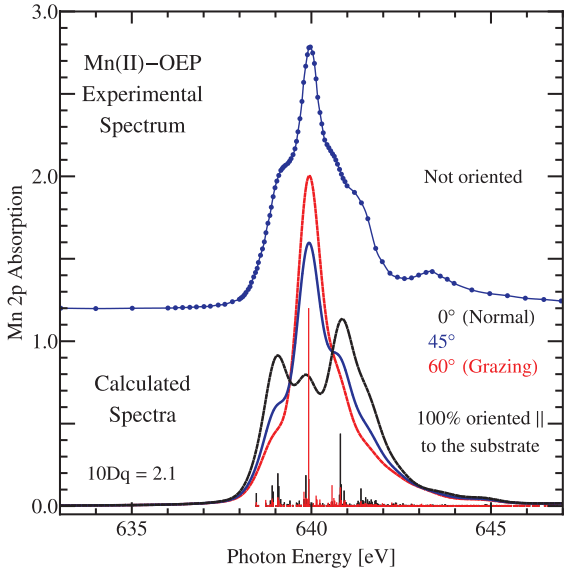

FIG. 8. Experimental and calculated spectra for Mn(II)-OEP. The data are from a thick sample, in which the molecules are no longer ordered. Such a disordered situation is comparable to a spectrum calculated for a 45° incident angle. Dramatic changes in the shape of the calculated spectra with the polarization angle might explain the large variation of relative peak heights observed in Mn-OEP from differently prepared samples.

TABLE II. Crystal field parameters produced by DFT calculations and experimental fitting (see Figs. 4–8 for the corresponding spectra). (PBE) indicates the calculated parameters before rescaling.

	10Dq (±0.05)	Dt (±0.005)	Ds (±0.005)	Slater integral prefactor (±0.05)
Mn-OEP	2.10	0.139	0.110	0.72
(PBE)	2.59	0.232	0.443	
Fe-Pc	2.66	0.232	0.700	0.9
(PBE)	2.94	0.257	0.597	
Co-Pc	2.96	0.276	0.496	0.95
(PBE)	3.12	0.290	0.522	
Co-OEP	2.65	0.247	0.444	0.85
(PBE)	2.91	0.281	0.422	
Ni-Pc	2.27	0.224	0.374	0.75
(PBE)	3.03	0.298	0.498	
Ni-OEP	2.33	0.230	0.383	0.77
(PBE)	2.85	0.261	0.333	

expected, given the more complex structure of a Pc with its two inequivalent rings of N atoms surrounding the metal. A possible reason for the absence of the splitting in the multiplet calculation is the omission of ligand hole transitions.

To extend the systematics of the crystal field splitting towards the left of the 3d transition metal series we have also investigated the Mn 2p edge of Mn(II)-Pc, even though we were not able to obtain oriented films from either Mn-Pc or Mn-OEP. Figure 8 shows the experimental and calculated spectra for a sample of Mn(II)-OEP that did not exhibit polarization dependence, which shows that the molecules have no preferential orientation on the surface, likely due to the thickness of the samples as well as some possible decomposition from the higher sublimation temperature. As with the other OEPs, the calculated red and black spectra in Fig. 8 represent normal and grazing incidence, assuming a perfectly ordered sample with all Mn(II)-OEP molecules lying flat on the substrate. In addition, a spectrum calculated for 45° incidence is shown in blue. The same spectrum is also calculated for randomly oriented molecules. It proves to be the best match to the experimental spectrum. The dramatic difference between the spectra at normal and grazing incidence is particularly noteworthy, as it could potentially be mistaken for mixing with other oxidation states of Mn. This is of particular concern for Fe- and Mn-based molecules, which occur in both the 2+ and 3+ oxidation states.[1] For example, the oriented Mn(II) spectrum calculated for normal incidence resembles the spectrum of Mn(III) in random orientation (compare Refs. 1, 16, 52, and 54).

The crystal field parameters obtained for Mn(II)-Pc in Table II produce a crystal field splitting in Figure 2 that differs substantially from those of Fe, Co, and Ni. This indicates that the 3d electron chemistry changes near the middle of the 3d transition metal series. A possible cause might be the drop in electronegativity from Fe to Mn, which stabilizes higher oxidation states for Mn. Indeed, the 3d metals to the left of Mn in the periodic table are only found in oxidation states higher than the 2+ oxidation state investigated here. While a comparable analysis of the crystal field has not been performed for Cr- and V-based porphyrins[33,34] and phthalocyanines, there are crystal field parameters available for TiO(IV)-phthalocyanines.[3,32] To be in the stable 4+ oxidation state, Ti-based phthalocyanines require additional axial ligands. Those affect the ordering of the $x^2 - y^2$ and z^2 levels, depending on the detailed arrangements of the axial ligands (see Fig. 7 in Ref. 3).

IV. CONCLUSIONS

This work investigates the trend of the crystal field splitting along the row of 3d transition metal phthalocyanines and porphyrins, in order to systematically improve dye molecules for solar cells. Polarization-dependent X-ray absorption spectroscopy, DFT, and multiplet calculations are used to determine the crystal field parameters 10Dq, Ds, and Dt. The detection of the polarization dependence of the 2p-to-3d multiplets is found to be very valuable for an unambiguous determination of the crystal field parameters. It provides both a scaling factor for calculated crystal field parameters and the symmetry of the transitions. Several DFT functionals were tested, and the PBE functional was found to be closest to the optimum fit. The PBE crystal field parameters still must be reduced somewhat, typically 5%–30%. Nevertheless, the DFT calculations are essential for producing accurate ratios of the crystal field parameters and thereby greatly reducing ambiguities in choosing starting values for the fit parameters. Additionally, DFT calculations are needed for an accurate picture of ground state electron occupancy, which determines the partially filled or empty states that are available for optical transitions.

This analysis reveals systematic trends in the splitting of the 3d levels for transition metal phthalocyanines and porphyrins in the 2+ oxidations state. The cross-over to transition metals with higher oxidation states to the left of Mn is discussed as well. Understanding the systematics of the crystal field in such metal-organic dye molecules is essential for steering photoexcited electrons in the right direction for optimal charge separation in solar cells.

ACKNOWLEDGMENTS

This work was supported by the NSF under Award Nos. CHE-1026245 and DMR-1121288 (MRSEC), and by the DOE under Contract No. DE-FG02-01ER45917 (ALS end station). The Advanced Light Source is supported by the Director, Office of Science, Office of Basic Energy Sciences, of the U.S. Department of Energy under Contract No. DE-AC02-05CH11231. P. L. Cook, C. K. Kennedy, and N. J. Jersett acknowledge support from the University of Wisconsin System 2012-2013 Applied Research Grant. J. M. García-Lastra acknowledges support from the Spanish Ministry of Economy and Competitiveness under Project Nos. FIS2009-07083, FIS2010-21282-C02-01, and FIS2012-30996. The Synchrotron Radiation Center is primarily funded by the University of Wisconsin-Madison with supplemental support from facility users and the University of Wisconsin-Milwaukee.

[1]P. L. Cook, X. Liu, W. Yang, and F. J. Himpsel, J. Chem. Phys. **131**, 194701 (2009).
[2]J. M. García-Lastra, P. L. Cook, F. J. Himpsel, and A. Rubio, J. Chem. Phys. **133**, 151103 (2010).
[3]D. F. Pickup, I. Zegkinoglou, B. Ballesteros, C. R. Ganivet, J. M. García-Lastra, P. L. Cook, P. S. Johnson, C. Rogero, F. de Groot, A. Rubio, G. de la Torre, J. E. Ortega, and F. J. Himpsel, J. Phys. Chem. C **117**, 4410 (2013).
[4]P. S. Johnson, P. L. Cook, I. Zegkinoglou, J. M. García-Lastra, A. Rubio, R. E. Ruther, R. J. Hamers, and F. J. Himpsel, J. Chem. Phys. **138**, 044709 (2013).
[5]I. Zegkinoglou, M.-E. Ragoussi, C. D. Pemmaraju, P. S. Johnson, D. F. Pickup, J. E. Ortega, D. Prendergast, G. de la Torre, and F. J. Himpsel, J. Phys. Chem. C **117**, 13357 (2013).
[6]K. Simonov, A. Vinogradov, M. Brzhezinskaya, A. Preobrajenski, A. Generalov, and A. Klyushin, Appl. Surf. Sci. **267**, 132 (2013).
[7]M.-S. Liao and S. Scheiner, J. Chem. Phys. **114**, 9780 (2001).
[8]T. Kroll, R. Kraus, R. Schönfelder, V. Y. Aristov, O. V. Molodtsova, P. Hoffmann, and M. Knupfer, J. Chem. Phys. **137**, 054306 (2012).
[9]M. L. M. Rocco, K.-H. Frank, P. Yannoulis, and E.-E. Koch, J. Chem. Phys. **93**, 6859 (1990).
[10]P. S. Miedema, M. M. van Schooneveld, R. Bogerd, T. C. R. Rocha, M. Hävecker, A. Knop-Gericke, and F. M. F. de Groot, J. Phys. Chem. C **115**, 25422 (2011).
[11]S. Stepanow, P. S. Miedema, A. Mugarza, G. Ceballos, P. Moras, J. C. Cezar, C. Carbone, F. M. F. de Groot, and P. Gambardella, Phys. Rev. B **83**, 220401 (2011).
[12]S. Ahmadi, M. N. Shariati, S. Yu, and M. Göthelid, J. Chem. Phys. **137**, 084705 (2012).
[13]M. G. Betti, P. Gargiani, R. Frisenda, R. Biagi, A. Cossaro, A. Verdini, L. Floreano, and C. Mariani, J. Phys. Chem. C **114**, 21638 (2010).
[14]F. Petraki, H. Peisert, F. Latteyer, U. Aygül, A. Vollmer, and T. Chassé, J. Phys. Chem. C **115**, 21334 (2011).
[15]F. M. F. de Groot, J. C. Fuggle, B. T. Thole, and G. A. Sawatzky, Phys. Rev. B **42**, 5459 (1990).
[16]M. M. Grush, J. Chen, T. L. Stemmler, S. J. George, C. Y. Ralston, R. T. Stibrany, A. Gelasco, G. Christou, S. M. Gorun, J. E. Penner-Hahn, and S. P. Cramer, J. Am. Chem. Soc. **118**, 65 (1996).
[17]M. Grobosch, B. Mahns, C. Loose, R. Friedrich, C. Schmidt, J. Kortus, and M. Knupfer, Chem. Phys. Lett. **505**, 122 (2011).
[18]J. Åhlund, K. Nilson, J. Schiessling, L. Kjeldgaard, S. Berner, N. Mrtensson, C. Puglia, B. Brena, M. Nyberg, and Y. Luo, J. Chem. Phys. **125**, 034709 (2006).
[19]P. S. Miedema, S. Stepanow, P. Gambardella, and F. M. F. de Groot, J. Phys. Conf. Ser. **190**, 012143 (2009).
[20]P. S. Miedema and F. M. de Groot, J. Electron. Spectrosc. Relat. Phenom. **187**, 32 (2013).
[21]B. Thole, G. V. D. Laan, and P. Butler, Chem. Phys. Lett. **149**, 295 (1988).
[22]K. Nakamura, Y. Kitaoka, T. Akiyama, T. Ito, M. Weinert, and A. J. Freeman, Phys. Rev. B **85**, 235129 (2012).
[23]F. Petraki, H. Peisert, U. Aygl, F. Latteyer, J. Uihlein, A. Vollmer, and T. Chassé, J. Phys. Chem. C **116**, 11110 (2012).
[24]M. D. Kuz'min, A. Savoyant, and R. Hayn, J. Chem. Phys. **138**, 244308 (2013).
[25]K. Baberschke, J. Phys. Conf. Ser. **190**, 012012 (2009).
[26]A. Labarta, E. Molins, X. Viñas, J. Tejada, A. Caubet, and S. Alvarez, J. Chem. Phys. **80**, 444 (1984).
[27]T. Kroll, V. Y. Aristov, O. V. Molodtsova, Y. A. Ossipyan, D. V. Vyalikh, B. Buchner, and M. Knupfer, J. Phys. Chem. A **113**, 8917 (2009).
[28]S. Krasnikov, A. Preobrajenski, N. Sergeeva, M. Brzhezinskaya, M. Nesterov, A. Cafolla, M. Senge, and A. Vinogradov, Chem. Phys. **332**, 318 (2007).
[29]S. Stepanow, A. Mugarza, G. Ceballos, P. Moras, J. C. Cezar, C. Carbone, and P. Gambardella, Phys. Rev. B **82**, 014405 (2010).
[30]W. Chen, H. Huang, S. Chen, X. Y. Gao, and A. T. S. Wee, J. Phys. Chem. C **112**, 5036 (2008).
[31]K. A. Nguyen and R. Pachter, J. Chem. Phys. **118**, 5802 (2003).
[32]Y. Zhang, S. Wang, A. Demasi, I. Reid, L. F. J. Piper, A. Y. Matsuura, J. E. Downes, and K. E. Smith, J. Mater. Chem. **18**, 1792 (2008).
[33]Y. Zhang, T. Learmonth, S. Wang, A. Y. Matsuura, J. Downes, L. Plucinski, S. Bernardis, C. O'Donnell, and K. E. Smith, J. Mater. Chem. **17**, 1276 (2007).
[34]Y. Zhang, S. Wang, T. Learmonth, L. Plucinski, A. Matsuura, S. Bernardis, C. ODonnell, J. E. Downes, and K. E. Smith, Chem. Phys. Lett. **413**, 95 (2005).
[35]J. Mack, and M. J. Stillman, in *The Porphyrin Handbook*, edited by K. M. Kadish, K. M. Smith, and R. Guilard (Elsevier Science, 2003), Vol. 16, Chap. 103, pp. 44–116.
[36]M. Atanasov, C. A. Daul, M.-M. Rohmer, and T. Venkatachalam, Chem. Phys. Lett. **427**, 449 (2006).
[37]M. J. Stillman and A. J. Thomson, J. Chem. Soc., Faraday Trans. 2 **70**, 790 (1974).
[38]F. de Groot, Coord. Chem. Rev. **249**, 31 (2005).
[39]E. Stavitski and F. M. de Groot, Micron **41**, 687 (2010).
[40]H. Ikeno, F. M. F. de Groot, E. Stavitski, and I. Tanaka, J. Phys. Condens. Matter **21**, 104208 (2009).
[41]H. Peisert, I. Biswas, M. Knupfer, and T. Chassé, Phys. Status Solidi B **246**, 1529 (2009).
[42]R. De Francesco, M. Stener, and G. Fronzoni, J. Phys. Chem. A **116**, 2885 (2012).
[43]G. te Velde, F. M. Bickelhaupt, E. J. Baerends, C. Fonseca Guerra, S. J. A. van Gisbergen, J. G. Snijders, and T. Ziegler, J. Comput. Chem. **22**, 931 (2001).
[44]S. H. Vosko, L. Wilk, and M. Nusair, Can. J. Phys. **58**, 1200 (1980).
[45]J. P. Perdew, K. Burke, and M. Ernzerhof, Phys. Rev. Lett. **77**, 3865 (1996).
[46]A. Trueba, P. Garcia-Fernandez, J. M. García-Lastra, J. A. Aramburu, M. T. Barriuso, and M. Moreno, J. Phys. Chem. A **115**, 1423 (2011).
[47]J. M. García-Lastra, J. Y. Buzaré, M. T. Barriuso, J. A. Aramburu, and M. Moreno, Phys. Rev. B **75**, 155101 (2007).
[48]B. N. Figgis and M. A. Hitchman, *Ligand Field Theory and Its Applications* (Wiley-VCH, New York, 2000).
[49]R. D. Cowan, *The Theory of Atomic Structure and Spectra* (University of California Press, Berkeley, CA, 1981).
[50]P. H. Butler, *Point Group Symmetry, Applications, Methods and Tables* (Plenum Press, New York, 1981).
[51]H. Ogasawara, A. Kotani, K. Okada, and B. T. Thole, Phys. Rev. B **43**, 854 (1991).
[52]S. P. Cramer, F. M. F. DeGroot, Y. Ma, C. T. Chen, F. Sette, C. A. Kipke, D. M. Eichhorn, M. K. Chan, and W. H. Armstrong, J. Am. Chem. Soc. **113**, 7937 (1991).
[53]O. Gunnarson, O. K. Andersen, O. Jepsen, and J. Zaanen, *Core-Level Spectroscopy in Condensed Systems*, Springer Series in Solid-State Sciences Vol. 81, edited by J. Kanamori and A. Kotani (Springer-Verlag, 1988), pp. 82–98.
[54]B. Gilbert, B. H. Frazer, A. Belz, P. G. Conrad, K. H. Nealson, D. Haskel, J. C. Lang, G. Srajer, and G. De Stasio, J. Phys. Chem. A **107**, 2839 (2003).
[55]See supplementary material at http://dx.doi.org/10.1063/1.4868552 for N 1s absorption spectra and polarization-dependence plots for Co(II)-Pc, Co(II)-OEP, Ni(II)-Pc, and Ni(II)-OEP. Also, calculated spectra are shown for Fe(II)-Pc as a function of the Slater parameter with fixed crystal field and as a function of the crystal field parameters with a fixed Slater parameter.